Hindawi Publishing Corporation
International Journal of Spectroscopy
Volume 2015, Article ID 572840, 15 pages
http://dx.doi.org/10.1155/2015/572840

Research Article

Raman Spectroscopy and Statistical Analysis of the Silicate Species and Group Connectivity in Cesium Silicate Glass Forming System

Armenak Osipov, Leyla Osipova, and Rimma Zainullina

Institute of Mineralogy of Ural Branch of RAS, Miass, Chelyabinsk Region 456317, Russia

Correspondence should be addressed to Armenak Osipov; armik@mineralogy.ru

Received 18 June 2015; Accepted 6 September 2015

Academic Editor: Hans Riesen

The Raman spectra of x%Cs_2O-$(100-x)$%SiO_2 (x = 17, 22, 27, 33, and 37 mol%) glasses and melts were measured in the temperature range of 293 to 1553 K. The concentrations of the Q^n species were calculated as a function of the composition and temperature based on the deconvolution analysis of the spectra. It was found that a dynamic equilibrium among structural units in the melts with $x > 17$ mol% can be described by disproportionation reaction $Q^3 \Leftrightarrow Q^4 + Q^2$. The enthalpy of this reaction was found to be equal to 32 ± 6, 43 ± 8, 56 ± 10, and 52 ± 9 for x = 22, 27, 33, and 37 mol%, respectively. The nonideal entropy of mixing (ΔS_{mix}) depends on the melt temperature and increases almost linearly with increasing temperature. The Q^n, Q^2–Q^2, and $Q^{n,ijkl}$ distributions with x ranging from 0 to 55 mol% were modeled using experimental data for the concentrations of the Q^n units.

1. Introduction

Knowledge of the structure of amorphous materials is fundamental for understanding of their physical and chemical properties. Structure-properties correlations of the silicate glasses and melts are of major importance in geochemical and technological fields. Therefore, an adequate understanding of the composition and temperature dependencies of glass and melt properties requires detailed information on their structure. Numerous studies of silicate glasses have demonstrated that silicon-oxygen tetrahedra with various numbers of bridging oxygen atoms are the fundamental structural blocks of these glasses. The silicon-oxygen tetrahedra are called Q^n units, where n = 0–4 is number of bridging oxygen atoms per SiO_4 tetrahedron. Schematic 2-dimensional representation of the Q^n species is shown in Figure 1(a). Q^n units form a continuous random network of glasses or silicate anions in melts via the Si-O-Si bridging linkages. The random network of SiO_2 glass consists of SiO_4 tetrahedra interconnected via their oxygen apexes, where all oxygen atoms are bridging (Q^4 units). The addition of alkali oxides to SiO_2 leads to the breaking of the Si-O-Si linkages and the formation of terminal oxygen atoms, each of which belongs only to one silicon atom, that is, the formation of Q^n species with $n < 4$ in the glass structure. Schematic representation of the formation of Q^n species with nonbridging oxygen atoms ($n < 4$) is shown in Figure 1(b). ^{29}Si MAS-NMR studies have shown that the concentrations of various types of Q^n units depend on the concentration of the modifier oxide and the type of alkali cation [1, 2]. Namely, the equilibrium

$$2Q^n \Longleftrightarrow Q^{n-1} + Q^{n+1} \quad (n = 3, 2, 1) \tag{1}$$

is shifted to the right with increasing cationic power of the metal cation (Z/r, where Z is the valency and r is the ionic radius, $Li^+ > Na^+ > K^+$). The Raman spectroscopy studies of rubidium and cesium silicate glasses [3, 4] allow the assertion that the above-mentioned regularity is valid for all alkali cations.

As known, equilibrium (1) ($n = 3$) is shifted to the right with increasing temperature in the case of the sodium and potassium silicate melts [5–12]. However, no significant changes in the local structure of lithium silicate melts were found [5, 12]. Moreover, thermodynamic calculations of

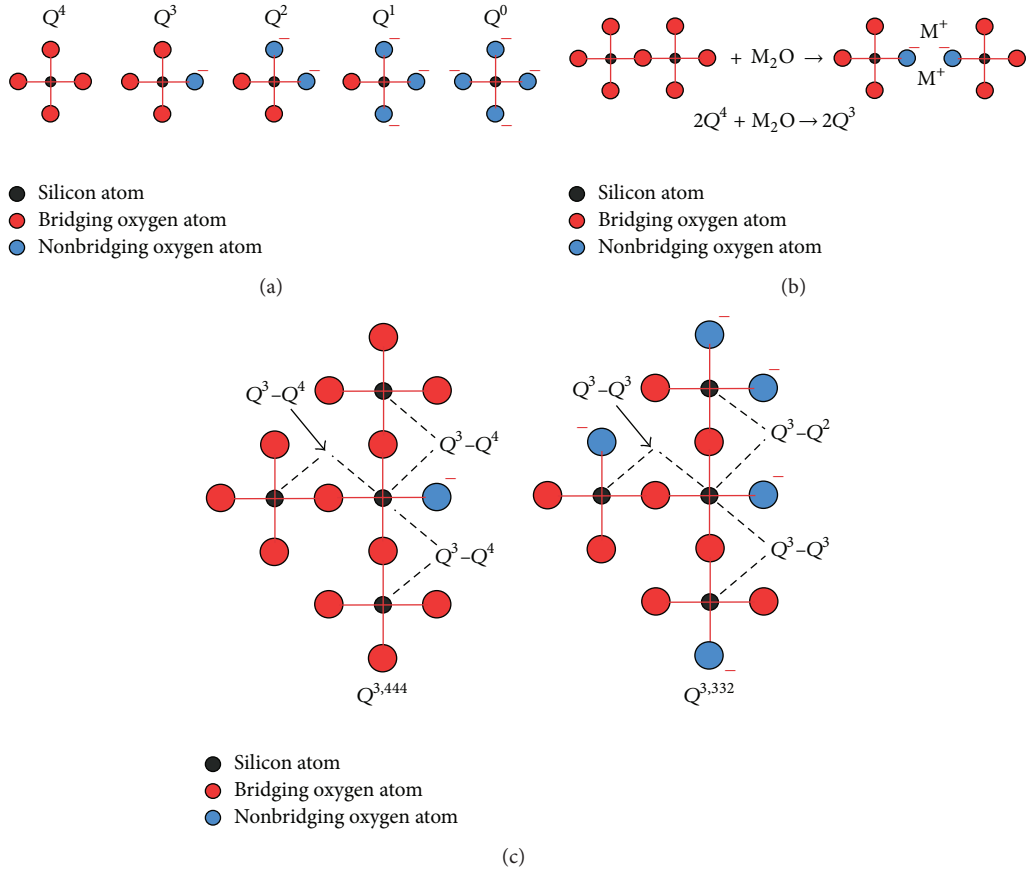

Figure 1: Schematic 2-dimensional representations of the Q^n species (a), of the formation of Q^n species with nonbridging oxygen atoms (b) and of some $Q^{n,ijkl}$ groups (c).

the Q^n distribution in the Li_2O-SiO_2 system have shown that equilibrium (1) is shifted to the left with increasing temperature, that is, towards an increase in the concentration of Q^3 units [7]. To the best of our knowledge, no data on the Q^n distribution and its changes with temperature in cesium silicate melts can be found in the literature. Therefore, the aim of this paper is a structural study of Cs_2O-SiO_2 glasses and melts by high-temperature Raman spectroscopy.

High-temperature Raman spectroscopy is a useful method for investigating not only the glass structure but also the melt structure over a wide temperature range [5–15]. As is known, the high-frequency region (800–1200 cm^{-1}) of the spectra of alkali silicate glasses and melts is characterized by a series of Raman bands originating from the Si-O^- stretching vibrations of various Q^n units. It is assumed that the intensities of these bands are proportionate to the concentrations of Q^n species [3, 5, 7, 8, 10–15]. Therefore, these bands can be used for the quantitative description of the structural changes of silicate glasses and melts depending on both the composition and temperature.

Although knowledge of the concentrations of Q^n species is important for describing the structure of silicate glasses and melts, it does not provide a clear idea of their structure, because the Q^n distribution provides no information about the interconnection between Q^n units. Currently, only a limited number of publications address this problem, and all of them focus on the Na_2O-SiO_2 system [6, 16–20]. Therefore, this paper studies this problem for Cs_2O-SiO_2 glasses and melts.

2. Material and Methods

2.1. Sample Preparation. Glass samples of the compositions $x\%Cs_2O$-$(100 - x)\%SiO_2$ (x = 17, 22, 27, 33, and 37 mol%) were prepared by the conventional melting and quenching method from reagent-grade SiO_2 and Cs_2CO_3. The initial reagents were dried (120°C, for 2 h), weighed, and mixed in the required ratios. The batch (5 g) was melted in a platinum crucible at t = 1000–1100°C for 2–5 h (depending on the melt composition) to obtain a bubble-free melt. The obtained melt was cooled directly in a platinum crucible in air at room temperature and then used for Raman measurements at various temperatures. To avoid glass hydration, Raman scattering measurements were started immediately after the sample preparation. It should be noted that due to the high viscosity of the $17\%Cs_2O$-$83\%SiO_2$ melt, we failed to prepare a bubble-free glassy sample. Thus this sample was only studied in the glassy state.

2.2. Raman Experiments. Raman scattering measurements were performed on a specially designed high-temperature apparatus, based on a DFS-24 double monochromator. To record the Raman spectra at different temperatures, the small platinum crucible was placed into a vertical compact electrical furnace. Thus, all spectra were recorded in 180° geometry. The operating temperature range was 20–1300°C and was controlled within ±1°C. The second-harmonic of an LTI-701 solid-state pulsed laser ($\lambda = 532$ nm, $\langle P \rangle = 500$ mW) operated at a modulation frequency of 8.7 kHz was used as the excitation source. The pulse duration of the acoustooptic switch was 2 μs. An uncooled FEU-79 photomultiplier was used to detect the Raman signal. A gated photon counting system was applied to minimize the thermal radiation signal. The spectral width of the slit was 6 cm^{-1} in all measurements. A detailed description of the experimental setup and recording conditions of the high-temperature Raman spectra can be found in [21–23].

To compare the spectra obtained at various temperatures, they were reduced to obtain the temperature- and frequency-dependent scattering intensity:

$$I_{\text{red}}(\nu) = I_{\text{obs}}(\nu)\left[1 - \exp\left(\frac{hc\nu}{kT}\right)\right]\frac{\nu\nu_0^3}{(\nu_0 - \nu)^4}, \quad (2)$$

where I_{obs} and I_{red} are the observed and reduced Raman intensities, respectively, ν and ν_0 are the Raman shift and wavenumber of the excitation source, respectively, and h, k, c, and T represent Planck's constant, Boltzmann's constant, speed of light, and temperature, respectively.

2.3. Simulation of the Q^n, Q^i–Q^j, and $Q^{n,ijkl}$ Distributions. As it is known, Zachariasen's rules [24] for glass formation are focused only on a local configuration of cation-oxygen polyhedra and their connectivity to each other (via corners, not edges or faces). Based on these rules it is possible to assume that the most important point in a modeling of a local structure of silicate glasses is a coordination number of glass-forming cations rather than a network dimensionality and topology as a whole. Any regular or random network where each node has four linkages with the nearest nodes and each bond joins only two nodes reproduces completely the Q^n distribution in pure SiO_2 (all structural units are Q^4). Formally, such network can be expressed in form of the table consisting of five lines and N columns, when N is a number of nodes in the system. Top line contains the serial number of node and other four lines contain the serial numbers of nodes which joined to the given in the top line. Thus, each column describes linkages between five nodes. Each node in this table was interpreted as a silicon atom and had four linkages with the nearest nodes. The bond between two nodes was interpreted as a Si-O-Si (hereafter we will use the abbreviation Q^i–Q^j) bridging bond (some examples of Q^i–Q^j bridging bonds are shown in Figure 1(c)). To calculate the Q^n distribution, it is necessary to break the preassigned number of bonds (the number of the bonds that must be broken is determined by the glass composition), and then the obtained configuration must be analyzed. In this approach, each node with n unbroken bonds and each broken bond were interpreted as a Q^n unit and a Si-O^{-+}M M^{+-}O-Si nonbridging bond, respectively. Three parameters, $1/w_1$, $1/w_2$, and $1/w_3$, were introduced into the modeling procedure to achieve the best agreement between the experimental Q^n concentrations and the calculated Q^n distribution. These parameters do not depend on the glass composition but do depend on temperature, and in addition to the concentration of various types of nodes, they determine the probability of the linkage break (Figure 2 demonstrates a role of these parameters in the computational algorithm). Taking into account the random character of the linkage choice and the table of linkages, 50 configurations were generated for each composition at a fixed temperature. The required concentrations of Q^n units were obtained by averaging of all 50 configurations of the table. The table was also analyzed to study the Q^i–Q^j (bridging bonds) and $Q^{n,ijkl}$ (group connectivity) distributions based on the Q^n distribution data (e.g., schematic 2-dimensional representations of the $Q^{3,444}$ and $Q^{3,332}$ groups are shown in Figure 1(c)). Here, n is the number of bridging oxygen atoms, and i, j, k, and l indicate the type of connected Q^n units. The modeling was performed in a composition range of 0 to 55 mol% Cs_2O content at two fixed temperatures (293 and 1223 K). A more detailed description of the modeling procedure can be found in [25, 26].

3. Results

3.1. Raman Spectra

3.1.1. Glass Spectra. The Raman spectra of glasses with the composition x%Cs_2O-(100 − x)%SiO_2 (x = 17, 22, 27, 33, and 37 mol%) are shown in Figure 3, in which the symbolic designations near the spectra (left side) indicate the Cs_2O content. The Raman spectra of glasses with relatively low Cs_2O contents (x = 17, 22, and 27 mol%) exhibit two bands with peak intensities at 510 and 598 cm^{-1}, one weak wide band at approximately 785 cm^{-1}, and a line at 1100 cm^{-1}, having the highest intensity in each spectrum, with a shoulder at 1150 cm^{-1}. The peak position at 510 cm^{-1} is gradually shifted toward higher frequencies and the 598 cm^{-1} line is slightly shifted toward lower frequencies with increasing Cs_2O content in the given composition range. In addition, the intensity of these bands increases, whereas the intensity of the weak line at 785 cm^{-1} decreases with the addition of cesium oxide. For the high-frequency envelope, the shape of this contour is most strongly affected by an increase in the modifier oxide content, which causes a gradual resolution deterioration of the 1100 and 1150 cm^{-1} bands and a drastic decrease in intensity for the high-frequency shoulder accompanied by an increase in the intensity of the 1100 cm^{-1} Raman band at $x >$ 27 mol%. The 1100 cm^{-1} line becomes more symmetric, and its width decreases. A new band at approximately 930 cm^{-1} distinguishes the 33Cs and 37Cs spectra from the $x <$ 33 mol% spectra. The intensity of this band increases with increasing x. It also should be noted that the intensity of the 510–530 cm^{-1} band is greater than that of the 598 cm^{-1} band at $x \leq 27$ mol%, and $I_{510-530} < I_{598}$ at $x > 27$ mol%.

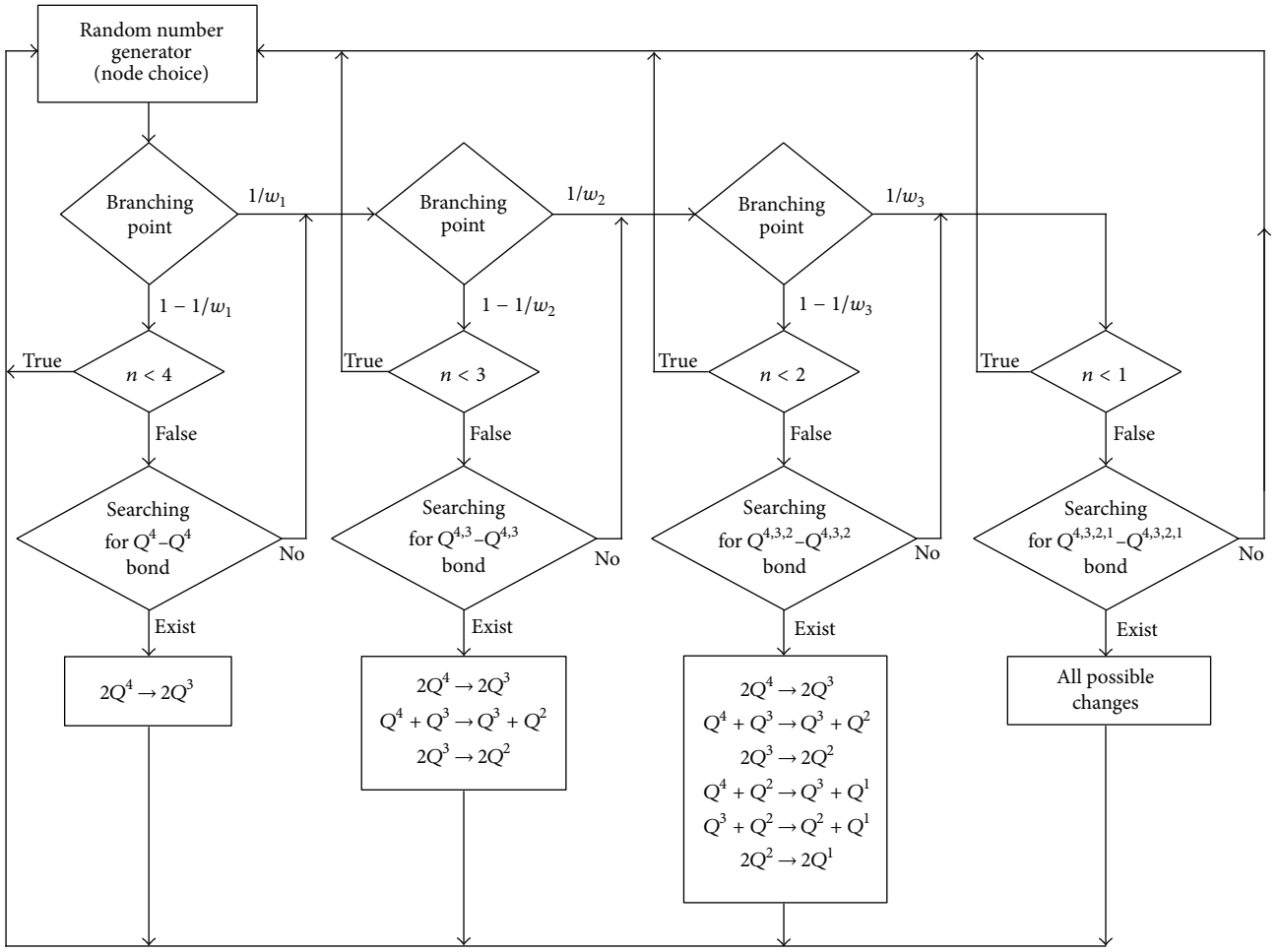

Figure 2: Block-diagram of simulation algorithm.

3.1.2. High-Temperature Raman Spectra. The Raman spectra of the 22%Cs_2O-78%SiO_2 and 27%Cs_2O-73%SiO_2 samples measured at different temperatures are shown in Figures 4(a) and 4(b). As seen in Figure 4(a), the peak intensity at 530 cm^{-1} decreases slightly and its position is gradually shifted toward lower frequencies with increasing temperature. The peak intensity at 598 cm^{-1}, in contrast to that of 530 cm^{-1} band increases with increasing temperature and remains at essentially the same frequency. No significant changes are observed in the peak intensity or the shape of the high-frequency envelope (1000–1200 cm^{-1}) at relatively low temperatures (up to ~898–1003 K). Only one symmetric wide line with maximum near 1100 cm^{-1} is observed in the high-frequency region at higher temperatures, and the intensity of this line decreases with increasing temperature. A new weak band at 930 cm^{-1} that appeared in the Raman spectra measured at temperatures above 1003 K is another peculiarity of the high-temperature spectra. All of the above-mentioned features of the changes in the 22Cs spectra with temperature are observed in the 27Cs spectra as well.

The Raman spectra of glasses and melts with modifier oxide contents of 33 and 37 mol% are shown in Figures 5(a) and 5(b), respectively. In contrast to the previous spectra, the line near 920–930 cm^{-1} is observed at all temperatures, and its intensity increases with temperature. This line is most clearly observed in the 37Cs spectra. The peak intensity at 1100 cm^{-1} obviously decreases with increasing temperature, and its position shifts slightly toward lower frequencies. In addition, the width of this band increases. The intensities of the low-frequency bands (520–530 and 598 cm^{-1}) depend weakly on temperature, but their width significantly increases with temperature. Finally, the formation of another new Raman line in the melt spectra with a maximum near 420 cm^{-1} should be noted (see Figure 5(b)). This line is observed in the previous spectra only as an unresolved low-frequency shoulder near the 530 cm^{-1} band.

3.2. Modeling Results. The results of the modeling of the Q^n and Q^i–Q^j distributions in the Cs_2O-SiO_2 system at two different temperatures (293 K, solid lines; 1223 K, dotted lines) are shown in Figures 6(a) and 6(b), respectively. In addition to our experimental data the literature data [1, 3, 27] on the concentrations of Q^n units in the Cs_2O-SiO_2 glasses and melts are also shown in Figure 6(a). As seen in this figure, the modeled curves well describe the experimental data for both glasses and melts over a wide compositions

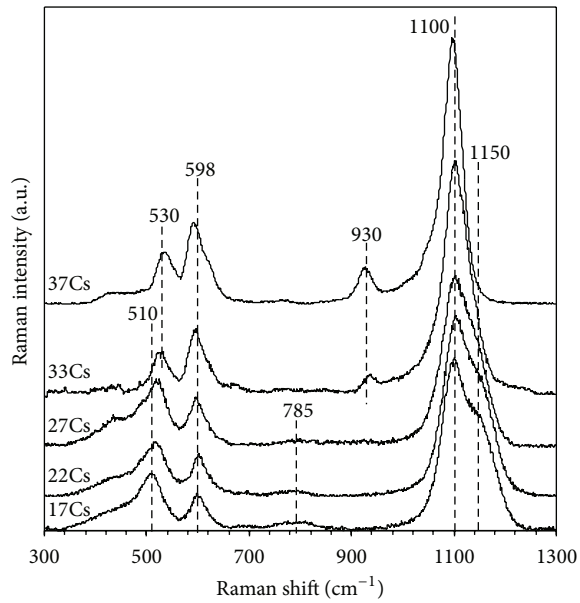

FIGURE 3: Raman spectra of x%Cs_2O-(100 − x)SiO_2 (x = 17, 22, 27, 33, and 37 mol%) glasses.

range. Temperature changes have no significant effect on the concentration of Q^n units in glasses and melts with relatively low Cs_2O contents (up to ~15 mol%) as well as in a narrow composition interval near 40 mol%. In turn, most considerable changes in the Q^n distribution are observed for samples with disilicate and metasilicate compositions. Here, the concentrations of the dominant type of structural units (Q^3 and Q^2 for disilicate and metasilicate, resp.) decrease with increasing temperature and are accompanied by an increase in the concentration of other structural units with n differing by ±1. In the aggregate, this phenomenon causes the curves describing the dependences of the Q^3 and Q^2 units on the composition to be slightly wider for the melts than for the glasses, but the positions of their maxima do not change with temperature.

As seen in Figure 6(b), only Q^i–Q^j bridging bonds with $|i - j| = 0$ or 1 may be observed in the system among all possibilities (Q^4–Q^4, Q^4–Q^3, Q^4–Q^2, Q^4–Q^1, Q^3–Q^3, Q^3–Q^2, Q^3–Q^1, Q^2–Q^2, Q^2–Q^1, Q^1–Q^1) of Q^i–Q^j bridging bonds. The maxima of the Q^i–Q^j curves decrease with increasing $|i - j|$ and are approximately the same for the Q^i–Q^j bonds with the same $|i - j|$ values. The maxima of the Q^4–Q^3 and Q^3–Q^2 curves depend weakly on temperature (approximately 1%), whereas the positions of these maxima are shifted toward higher Cs_2O concentrations. In addition, an increase in the width of these curves is also observed. The width and position of the peak of the Q^3–Q^3 and Q^2–Q^2 curves behave similarly, but their maxima decrease more dramatically with increasing temperature (approximately 20%). The Q^i–Q^j curves with $|i - j| = 2$ are shown in the inset to Figure 6(b). As observed, the dependence of the concentration of the given Q^i–Q^j bridges on temperature is opposite to that typical for Q^i–Q^j bridging bonds with $|i - j| = 0$. In this case, a significant increase in the Q^4–Q^2 and Q^3–Q^1 concentrations with increasing temperature is observed. Nevertheless, the concentration of these Si-O-Si bonds is low in both glass and melt and is less than 1% and 4% at 293 and 1223 K, respectively.

The modeling results of the concentrations of the $Q^{4,ijkl}$ and $Q^{3,ijk}$ groups as a function of composition at different temperatures (293 and 1223 K) are shown in Figures 7(a)–7(d). The concentrations were calculated in two ways: relative to the concentration of the appropriate type of structural unit (Figures 7(a) and 7(c) for $Q^{4,ijkl}$ and $Q^{3,ijk}$, resp.),

$$\left[Q^{n,ijkl}\right] = \frac{N_{Q^{n,ijkl}}}{N_{Q^n}} \times 100\%, \quad (3)$$

and relative to the total concentration of Q^n units (Figures 7(b) and 7(d) for $Q^{4,ijkl}$ and $Q^{3,ijk}$, resp.),

$$\left[Q^{n,ijkl}\right] = \frac{N_{Q^{n,ijkl}}}{\sum_{n=0}^{4} N_{Q^n}} \times 100\%. \quad (4)$$

In these equations, $N_{Q^{n,ijkl}}$ and N_{Q^n} are the amounts of different types of groups and structural units, respectively.

As seen in Figure 7(a), the gradual increase in concentration of the modifier oxide leads to the following transformations of the $Q^{4,ijkl}$ groupings: $Q^{4,4444} \rightarrow Q^{4,4443} \rightarrow Q^{4,4433} \rightarrow Q^{4,4333} \rightarrow Q^{4,3333} \rightarrow Q^{4,3332}$. In addition, $Q^{4,4432}$, $Q^{4,4332}$, and $Q^{4,3322}$ groups are also formed in the glass structure. As seen in the inset to Figure 7(a), however, their concentrations are lower than 7%. Both the coexistence regions and the variety of the $Q^{4,ijkl}$ groups are higher in melts than in glasses. The $Q^{4,4332}$, $Q^{4,3322}$, and $Q^{4,3222}$ groups supplement the list of $Q^{4,ijkl}$ groups at high temperature (1223 K). Their maximum concentration exceeds 7% in the melt structure and is low in the glasses. The $Q^{4,4322}$, $Q^{4,2222}$, $Q^{4,3221}$, $Q^{4,3331}$, and $Q^{4,3321}$ groups may also appear in the melt structure but their concentration is less than 7% (see Figure 7(a)). The shape of the $Q^{4,4444}(x)$, $Q^{4,4443}(x)$, and $Q^{4,4433}(x)$ curves depends slightly on temperature, whereas the $Q^{4,4333}(x)$, $Q^{4,3333}(x)$, and $Q^{4,3332}(x)$ curves are subject to dramatic changes. An increase in the width of the curves and a shift in the position of their maxima toward large x are typical for all of them. The ratio between the maxima of these curves at 293 K is

$$M_{Q^{4,3333}} > M_{Q^{4,4333}} \approx M_{Q^{4,4332}}, \quad (5)$$

and that at 1223 K is

$$M_{Q^{4,3332}} > M_{Q^{4,4333}} > M_{Q^{4,3333}}. \quad (6)$$

The region of existence of the $Q^{3,ijk}$ groups is somewhat broader than that of $Q^{4,ijkl}$ and extends to $x \approx 52$ mol% (see Figure 7(c)). The transformation of $Q^{3,ijk}$ groups, depending on x, can be represented by the sequence $Q^{3,444} \rightarrow Q^{3,443} \rightarrow Q^{3,433} \rightarrow Q^{3,333} \rightarrow Q^{3,332} \rightarrow Q^{3,322} \rightarrow Q^{3,222} \rightarrow Q^{3,221}$. In addition, some amount of $Q^{3,432}$ groups (less than 3% of the total amount of Q^3 units) and $Q^{3,321}$ groups (less than 4%) can exist in the glass structure with disilicate and metasilicate

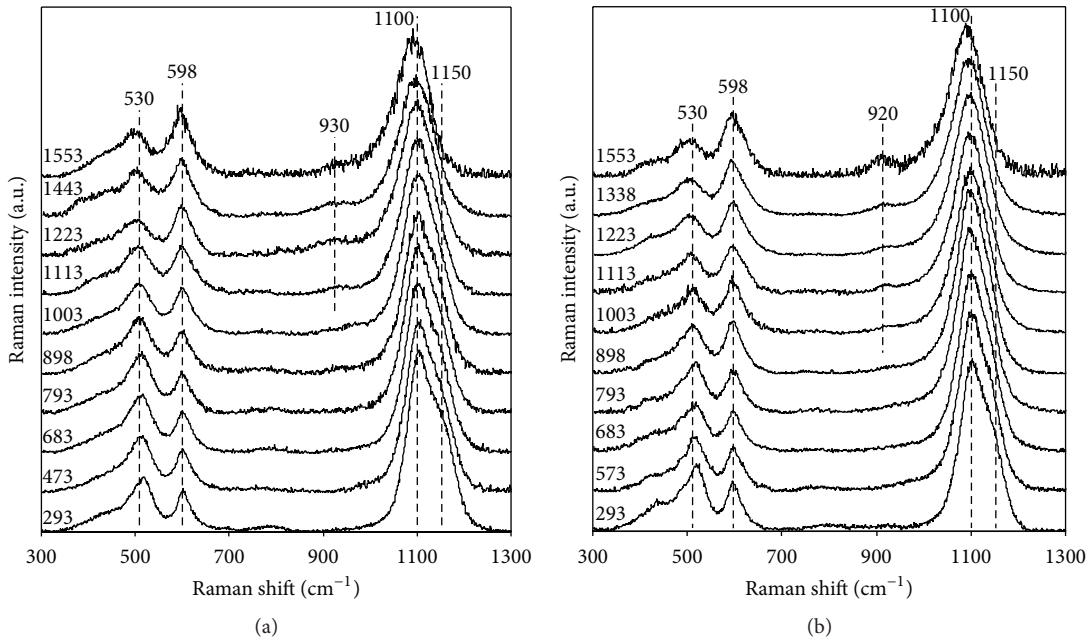

FIGURE 4: Low- and high-temperature Raman spectra of the 22%Cs_2O-78%SiO_2 (a) and 27%Cs_2O-73%SiO_2 (b) glasses and melts (hereinafter a temperature of the samples is shown in K).

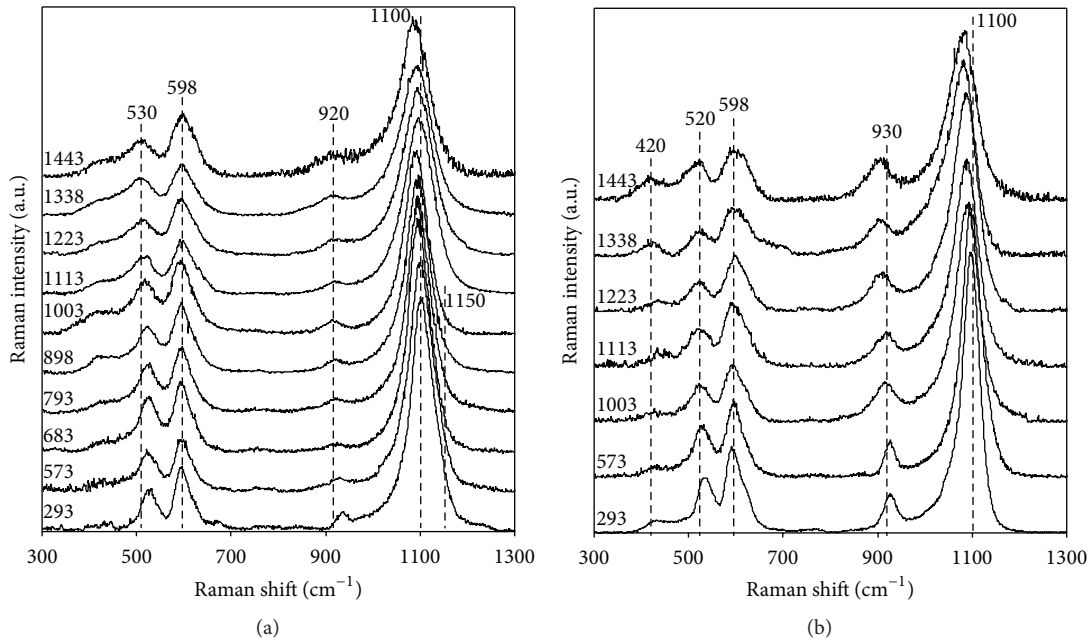

FIGURE 5: Low- and high-temperature Raman spectra of the 33%Cs_2O-67%SiO_2 (a) and 37%Cs_2O-63%SiO_2 (b) glasses and melts.

compositions, respectively (see the inset in Figure 7(c)). The region of coexistence of the $Q^{3,ijk}$ groups increases by ~2.5% and reaches 55% as the temperature increases up to 1223 K. It is also accompanied by an increase in the width of the $Q^{3,ijk}(x)$ curves, a shift of the maxima of these curves toward large x values, and the leveling of their maxima. The concentration of the dominant type of structural group (at a given composition) decreases and the fraction of the $Q^{3,ijk}$ groups that are untypical for glass increases with increasing temperature. As before, no significant changes are observed in the $Q^{3,ijk}$ distribution at $x < 20$ mol%.

The $Q^{2,ij}$ and $Q^{1,i}$ distributions calculated according to (3) and (4) are shown in Figures 7(a)–7(d). Figures 8(a) and 8(c) represent the $Q^{2,ij}$ and $Q^{1,i}$ distributions relative to the Q^2 and Q^1 contents, respectively, and Figures 8(b) and 8(d) represent the concentrations of the $Q^{2,ij}$ and $Q^{1,i}$ groups relative to the

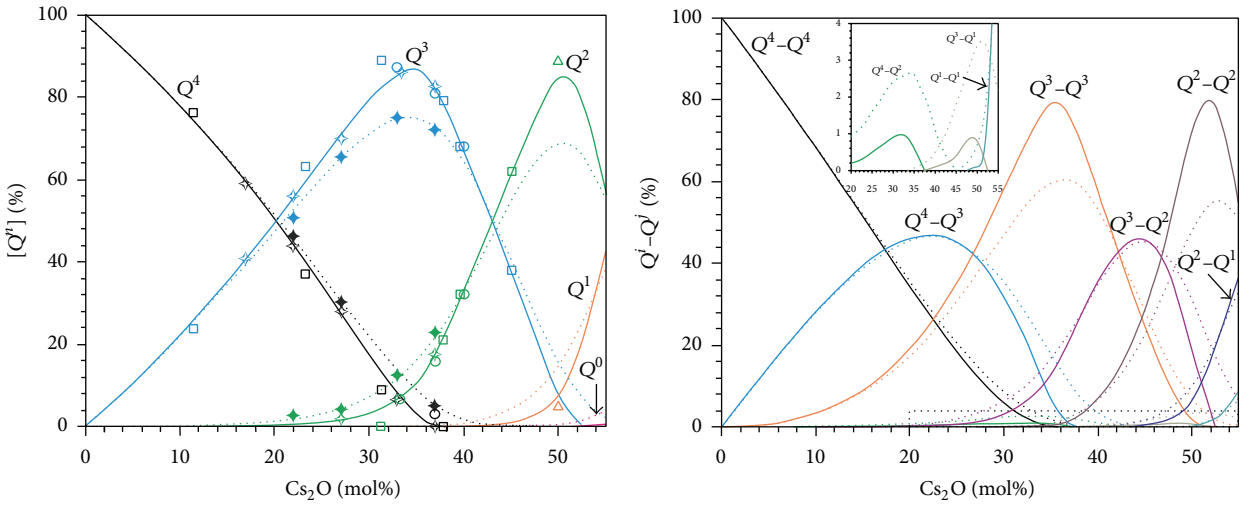

FIGURE 6: Q^n (a) and Q^i–Q^j (b) distributions for glasses (solid lines, $T = 293$ K) and melts (dotted lines, $T = 1223$ K) of Cs_2O-SiO_2 system. Symbols are experimental data (□: [1], ◯: [3], △: [27], and ✦: this work).

total amount of Q^n units, respectively. As seen in Figure 8(a), an increase in concentration in the modifier oxide leads to the transformation of the $Q^{2,ij}$ groups in the following sequence: $Q^{2,44} \rightarrow Q^{2,43} \rightarrow Q^{2,33} \rightarrow Q^{2,32} \rightarrow Q^{2,22} \rightarrow Q^{2,21} \rightarrow Q^{2,11}$. It should be noted that the concentration of the $Q^{2,44}$ and $Q^{2,43}$ groups relative to Q^n units in the glass structure is low at $x > 15$ mol% (less than 1.5%; see Figure 8(b)), although their fraction relative to the total amount of $Q^{2,ij}$ groups exceeds 40%. Moreover, the $Q^{2,ij}$ groups are only formed in the glass structure in an amount exceeding 1% at $x > 28$ mol%, as follows from Figure 8(b). As before, an increase in the width of the $Q^{2,ij}(x)$ curves and a shift in the position of their maxima toward large x values are observed with increasing temperature. The $Q^{2,ij}(x)$ maxima change such that the difference between maxima decreases with increasing temperature.

The $Q^{1,i}$ distribution has the simplest form, which is evidently related to the low variety of such groups. (A change in i from 4 to 1 gives only four types of $Q^{1,i}$ groups.) The concentration of the $Q^{1,4}$ groups is negligible in the glass structure. Therefore, a consequence of the transformations of the $Q^{1,i}$ groups looks similar to $Q^{1,3} \rightarrow Q^{1,2} \rightarrow Q^{1,1}$. The data presented in Figures 8(c) and 8(d) support the assumption that the changes in the $Q^{1,i}(x)$ curves will be similar to those described above.

4. Discussion

4.1. Raman Spectra and Structure of the x%Cs_2O-$(100 - x)SiO_2$ (x = 17, 22, 27, 33, and 37 mol%) Glasses. It is rational to divide the overall frequency range into low-frequency (400–700 cm^{-1}) and high-frequency (800–1200 cm^{-1}) intervals to analyze the obtained Raman spectra. The low-frequency interval is related to the stretching and some of the bending vibrations of Si-O-Si linkages. Two narrow lines (490 cm^{-1} (D_1) and 602 cm^{-1} (D_2)) along with a broad intense line (~450 cm^{-1}) are observed in the Raman spectrum of g-SiO_2 (e.g., [28]). It is accepted that the D_1 and D_2 lines can be related to the symmetric oxygen breathing vibration of three- (D_2) and four-membered (D_1) siloxane rings, consisting of SiO_4 tetrahedra [28–32]. The investigation of the Raman spectra of alkali silicate glasses with high SiO_2 content [33] has shown that the bands near 490 and 602 cm^{-1} are gradually shifted toward higher and lower frequencies, respectively, with increasing Cs_2O content. Thus, it can be assumed that the Raman bands near 510–530 and 598 cm^{-1} in our spectra have the same origin as the D_1 and D_2 lines, respectively. The change in the intensity of these lines as a function of glass composition (see Figure 3) shows that the increase in modifier oxide concentrations leads to changes in the statistical distribution of n-membered rings, wherein the concentration of three-membered rings gradually increases. This observation is in accordance with the results published in [27], where an increase in concentrations of three-membered rings with increasing Cs_2O was shown based on NMR data. The concentration of the four-membered rings changes weakly at $17\% < x < 22\%$ and decreases at higher Cs_2O content.

The Raman bands originating from the symmetric stretching vibration of the Si-O^- terminal groups of various Q^n ($n < 4$) units are located in the high-frequency range of spectra of alkali silicate glasses [34]:

(i) the band at 1050–1100 cm^{-1} is due to the symmetric stretching vibrations of the terminal oxygen atoms of SiO_4 tetrahedra with one nonbridging oxygen (NBO) atom, that is, Q^3 units;

(ii) the band at 920–950 cm^{-1} results from the Si-O^- stretching of SiO_4 tetrahedra with two NBO (Q^2 units);

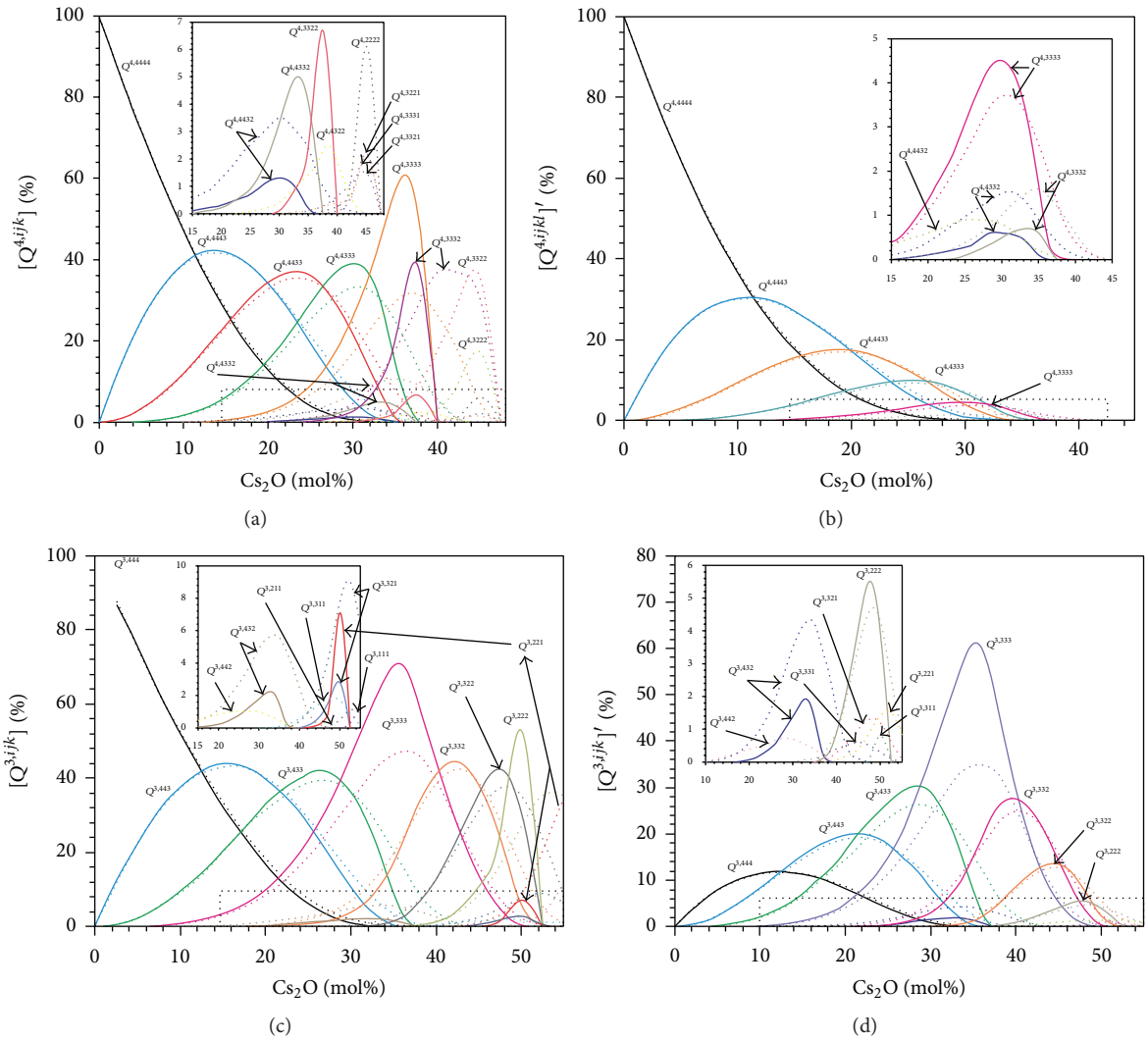

FIGURE 7: $Q^{4,ijkl}$ ((a) and (b)) and $Q^{3,ijk}$ ((c) and (d)) distributions in Cs_2O-SiO_2 glasses (solid lines, T = 293 K) and melts (dotted lines, T = 1223 K). ((a) and (c) equation (3); (b) and (d) equation (4)).

(iii) the Raman band near 900 cm^{-1} is attributed to the stretching vibration of the Q^1 units (SiO_4 tetrahedra with three NBO);

(iv) finally, the line at 850 cm^{-1} is related to the symmetric stretching mode of Q^0 anions.

As seen in Figure 3, only the 1050–1100 and 930 cm^{-1} bands are observed in the Raman spectra of studied glasses. It should be noted that the 1050–1100 cm^{-1} band exists in all spectra, whereas the 930 cm^{-1} band is only observed in the spectra of glasses with relatively high Cs_2O contents (33Cs and 37Cs). In addition, a high-frequency shoulder with maximum at approximately 1150 cm^{-1} is observed in the Raman spectra of the 17Cs, 22Cs, and 27Cs samples. Although alkali silicate glasses have been studied for a long time, a review of the literature revealed that the origin of this shoulder is still controversial. In one series of publications [12, 13, 35], the 1150 cm^{-1} line was attributed to the Si-O stretching vibration in fully polymerized structural species, that is, the vibrations of Q^4 units. However, based on a study of the Raman spectra of alkali silicate glasses with various compositions Matson et al. [33] have suggested that this line may be assigned to the vibrations of the $Q^{3\prime}$ units, which are structurally and vibrationally distinguished from those of the Q^3 units, producing the 1050–1100 cm^{-1} band. They argued that the 1150 cm^{-1} shoulder has significantly greater intensity than could reasonably be assigned to residual g-SiO_2 spectral features. In addition, they found no correlation between the intensity of this band and other bands (e.g., 450 cm^{-1}) characteristic of the g-SiO_2 spectrum. Based on these conclusions, the 1150 cm^{-1} shoulder was attributed to $Q^{3\prime}$ units, which have slightly stronger (shorter) Si-O^- bond than the one producing the 1100 cm^{-1} line [33].

Matson et al.'s assumption concerning the origin of the 1150 cm^{-1} shoulder was confirmed later on by You with co-authors [6]. The correlation between the Raman shift and connecting topology of adjacent Q^n units was found based

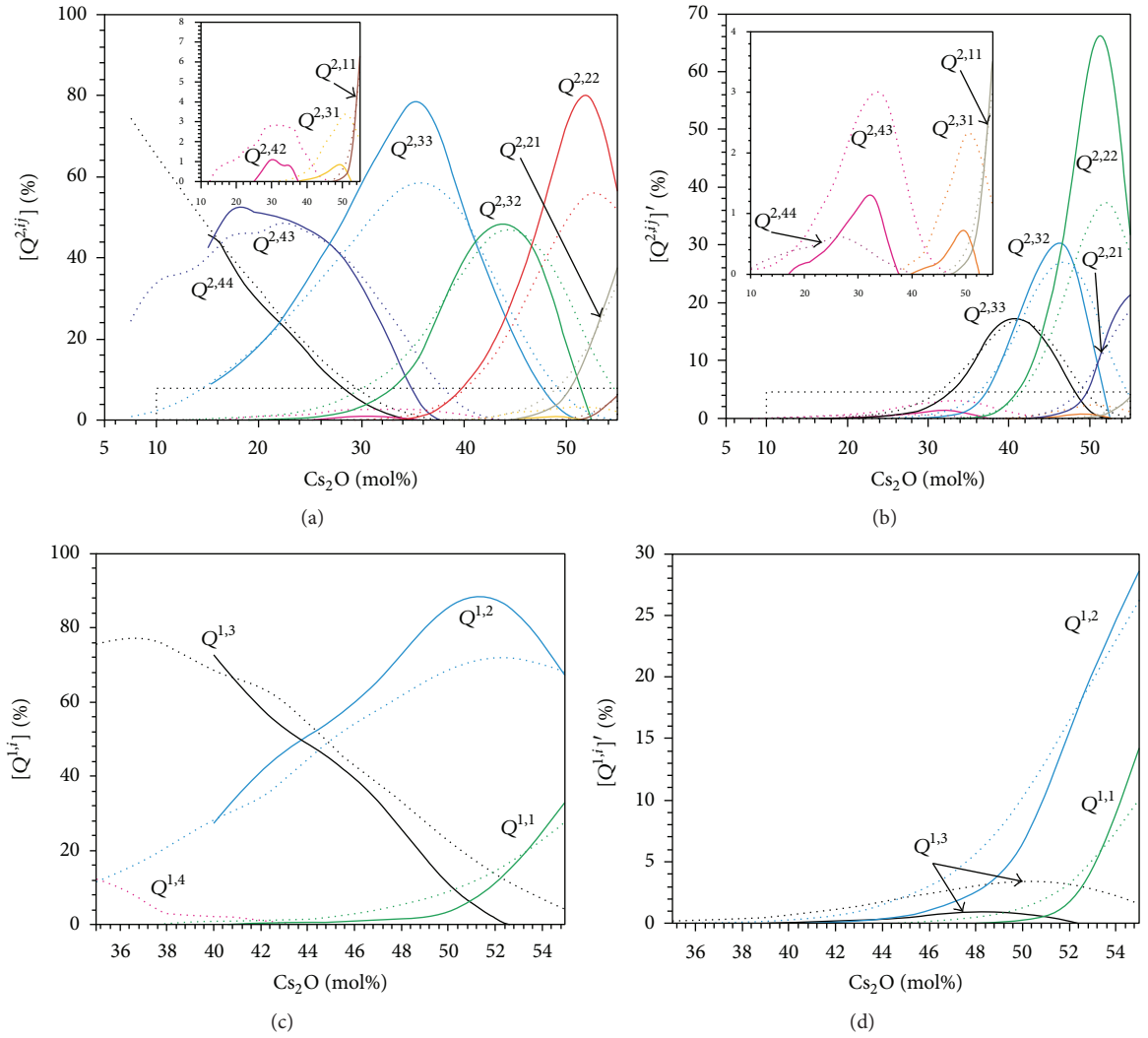

FIGURE 8: $Q^{2,il}$ ((a) and (b)) and $Q^{1,i}$ ((c) and (d)) distributions in Cs_2O-SiO_2 glasses (solid lines, T = 293 K) and melts (dotted lines, T = 1223 K). ((a) and (c) equation (2); (b) and (d): equation (3)).

on the quantum chemical calculation of the characteristic frequencies of Q^n species. In other words, it was demonstrated that the Raman shift of the symmetric stretching vibration of Q^n units decreases as the number of bridging oxygen atoms of the nearest-neighbor Q^n species adjacent to the given Q^n unit decreases. For example, the Raman shift of the $Q^{3,444}$ group is higher than that of the $Q^{3,333}$ group. In our opinion, the conclusions in [6] are strong evidence of Matson's assumption. Thus, we will rely on Matson's interpretation of the origin of 1150 cm^{-1} band in our paper.

The qualitative examination of the Raman spectra of Cs_2O-SiO_2 glasses (Figure 3) confirms that the structure of glasses with a Cs_2O content below 33 mol% consists of Q^4 and Q^3 units (the existence of Q^4 units is obvious and requires no evidence, although the 1150 cm^{-1} shoulder indirectly proves the presence of such structural units) and that the Q^3 species are present, at the least, in the form of $Q^{3,444}$ and $Q^{3,333}$ groups. The Raman band at 930 cm^{-1} shows that Q^2 units are formed in the 33Cs and 37Cs glasses. The presence of Q^4 units in the structure of disilicate glasses is a result of satisfying the charge balance (NBO/Si = 1). Regarding the 37Cs glass, the presence of Q^4 species can be identified only by the quantitative analysis of the corresponding spectrum.

The high-frequency envelope (800–1300 cm^{-1}) of the registered Raman spectra was simulated as a superposition of the Gaussian lines to estimate the Q^n concentrations. The number of Gaussian lines was sufficient to reproduce the original spectra with a correlation factor of ≥0.98. The interpretation of the Raman bands described above was also taken into account. In addition, some results published in [6] were also taken into account: Q^n species with equal n give more than one band and peak position of individual band depends on the structural position of Q^n units. For example, wavenumbers of NBO symmetric stretching vibration of Q^3 species are located in the range of 1050 to 1150 cm^{-1}, whereas Q^2 units give a set of the individual peaks in the range of

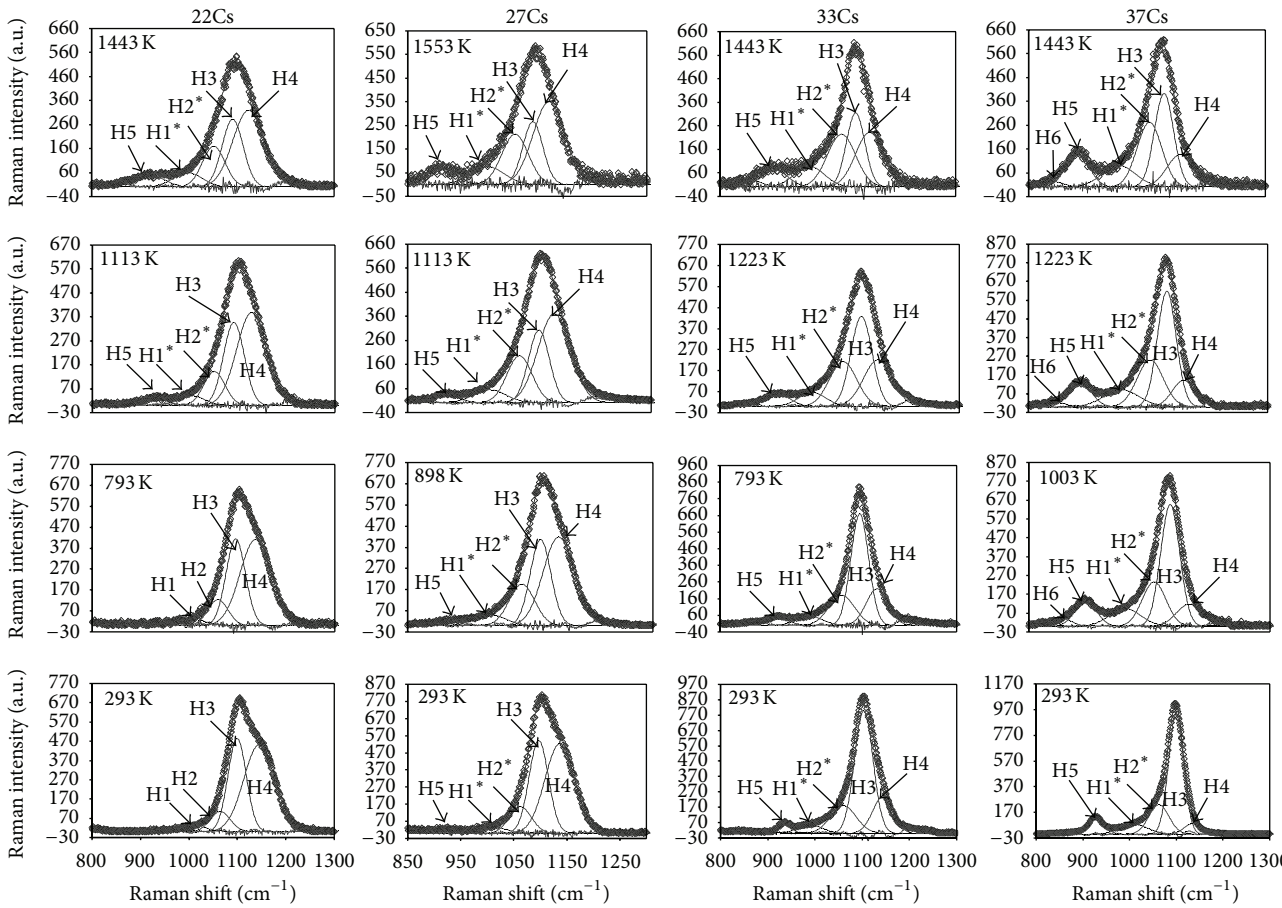

FIGURE 9: Examples of the band deconvolution of Cs_2O-SiO_2 glasses and melts Raman spectra between 800 and 1300 cm^{-1}.

930 to 1050 cm^{-1} [6]. Several examples of the deconvolution results of the Raman signal of the studied samples in the high-frequency region are shown in Figure 9. Four Gaussian lines were sufficient to reproduce the low-temperature (293 K) Raman spectra of the 17Cs and 22Cs glasses, whereas five lines were needed to simulate the 27Cs, 33Cs, and 37Cs spectra. The H3 and H4 bands were attributed to the Q^3 species. Because the 17Cs and 22Cs glasses consist of Q^4 and Q^3 units, it is possible to assume that only four types of structural groups ($Q^{3,444}$, $Q^{3,443}$, $Q^{3,433}$, and $Q^{3,333}$) can exist in structure of these glasses. Considering the dependence of the Raman shift of $Q^{3,ijk}$ groups on the i, j, and k indexes established in [6], it was assumed that the $Q^{3,444}$ and $Q^{3,443}$ groups are the main contributors to the intensity of the H4 band and that the vibrations of the $Q^{3,433}$ and $Q^{3,333}$ groups are the main contributors to the intensity of the H3 band. This qualitatively agrees with the simulation results of the $Q^{3,ijk}$ distribution represented in Figures 7(c) and 7(d). The H2 band is most likely due to the stretching vibrations of the Si-O-Si linkages [3, 31]. The origin of the H1 line is unclear. It is possible that this line is a result of the assumption of the Gaussian shape of the elementary bands in the spectra of glasses with relatively low Cs_2O concentrations (17Cs and 22Cs); that is, this line is an error in the choice of the type of elementary bands. The relative area of the H1 band is the same for the 17Cs and 22Cs spectra (0.02) and its intensity increases with further increases in the Cs_2O content. The H2 line behaves similarly. An increase in intensity of both H1 and H2 lines begins from the appearance of a new H5 line in the deconvolution of the Raman spectra. The H5 line indicates the formation of Q^2 species in the structure of the samples. According to [6], it is possible to assume that the vibrations of the $Q^{3,ijk}$ groups, connected with one or two Q^2 units, for example, $Q^{3,332}$ and $Q^{3,322}$ groups, also contribute to the intensity of the H2 band at higher concentrations of the modifier oxide. Thus, the 1060 cm^{-1} line was designated as H2* in the deconvolution of the 27Cs, 33Cs, and 37Cs spectra. In turn, the H1* line can be attributed to the vibrations of the $Q^{2,44}$, $Q^{2,43}$, and $Q^{2,33}$ groups according to the $Q^{2,ij}$ distribution represented in Figures 8(a) and 8(b). Finally, the H5 line was ascribed to $Q^{2,32}$ groups.

The localized nature of the silicon-oxygen stretching motions of silicate units, containing SiO_4 tetrahedra with one, two, three, or four nonbridging oxygen atoms [34, 36] allows us to use the relative integral intensities of the Gaussian components to calculate the Q^n concentrations.

If three types (Q^4, Q^3, Q^2) of Q^n species coexist in a structure simultaneously, then their concentrations

($[Q^4]$, $[Q^3]$, $[Q^2]$) can be obtained from the following system of equations:

$$\begin{aligned} \left[Q^4\right] + \left[Q^3\right] + \left[Q^2\right] &= 1, \\ \left[Q^3\right] + 2\left[Q^2\right] &= \frac{2x}{1-x}, \\ \left[\frac{Q^3}{Q^2}\right] &= a\frac{I_{\mathrm{H2}^*} + I_{\mathrm{H3}} + I_{\mathrm{H4}}}{I_{\mathrm{H1}^*} + I_{\mathrm{H5}}}. \end{aligned} \tag{7}$$

The coefficient proportionality, a, was chosen to achieve a best accordance with data published in other papers [3, 4]. Furthermore, if there is reason to believe that Q^2 units are absent in the glass structure (as in the 17Cs and 22Cs glasses), then the final equation does not make sense and the $[Q^4]$ and $[Q^3]$ concentrations can be calculated analytically from the first two equations without any experimental data. Considering the complicated nature of the H1* and H2* bands, two scenarios were calculated. In the first variant, the I_{H2^*} and I_{H1^*} values were equal to the areas of the H2* and H1* components, respectively. The integral intensity of the H1* and H2* bands was reduced on the $\langle I_{\mathrm{H1}}\rangle$ and $\langle I_{\mathrm{H2}}\rangle$ values in the second scenario. Here, $\langle I_{\mathrm{H1}}\rangle$ and $\langle I_{\mathrm{H2}}\rangle$ are the average values of the integral intensities of the H1 and H2 bands, respectively, measured from the deconvolution results of the high-frequency range of the Raman spectra of low-alkali glasses (17Cs and 22Cs). The peak positions, relative areas of the partial bands, and the $[Q^n]$ concentrations calculated according to system (4) are summarized in Table 1. The peak positions and FWHM values were established within $\pm 5\,\mathrm{cm}^{-1}$. As seen in the table, the first calculation variant yields slightly higher $[Q^4]$ and $[Q^2]$ concentrations and a somewhat lower $[Q^3]$ value. The calculation results of the second scenario yields the opposite trend. Accounting for the $\langle I_{\mathrm{H1}}\rangle$ and $\langle I_{\mathrm{H2}}\rangle$ values produces higher $[Q^3]$ values and somewhat lower concentrations of Q^4 and Q^2 units. The greatest difference between the calculation results is observed for the 27Cs glass and is ≈3% for the $[Q^3]$ concentration.

4.2. High-Temperature Raman Spectra and Structure of the Cs_2O-SiO_2 Glasses and Melts. The Raman spectra of the 22Cs sample measured in the temperature range of 293 to 1553 K are shown in Figure 4(a). As seen from this figure, the change in temperature results in changes in the spectra in both low- and high-frequency ranges. According to the above-mentioned structural interpretation of the Raman bands, the significantly greater intensity of the $598\,\mathrm{cm}^{-1}$ band and significantly lower intensity of the $530\,\mathrm{cm}^{-1}$ band in the melt spectra in comparison with the glass spectra indicate a considerable influence of temperature on the distribution of n-membered rings. These data support the assumption that the fraction of 4-membered rings decreases and fraction of 3-membered rings increases with increasing temperature. In turn, the changes in the shape of the high-frequency envelope and the appearance of a weak Raman signal at $930\,\mathrm{cm}^{-1}$ in the melt spectra (this band is absent in the glass spectrum) point to a structural transformation in the local structure of the sample. It can be argued at a qualitative level that the list of structural units for glasses and melts will differ. The local structure of the glassy sample includes only two structural units, Q^4 and Q^3, whereas that of melts contains significant amounts of Q^2 units ($930\,\mathrm{cm}^{-1}$ line). The same conclusions may be drawn from the 27Cs spectra (Figure 4(b)). Changes in the I_{598}/I_{530} ratio and the gradual increase in the intensity of the 920–930 cm^{-1} band also occur. Such obvious changes in the low-frequency range are not observed in the Raman spectra of samples with higher Cs_2O contents (see Figures 5(a) and 5(b)). In this case, it is difficult to derive well-defined conclusions about dependence of the distribution of the n-membered rings on temperature. At the same time, an increase in the intensity of the 920–930 cm^{-1} band and a decrease in the intensity of the 1090–1100 cm^{-1} band are observed with increasing temperature, as before. Thus, an increase in temperature leads to a decrease in the concentration of the Q^3 units and an increase in the fraction of the Q^2 species in all studied samples.

The high-frequency range of the Raman spectra measured at different temperatures was simulated as a superposition of the Gaussian lines to study the influence of temperature on the concentrations of Q^n species (see Figure 9). The parameters of the partial bands obtained from the modeling of glass spectra were used in the deconvolution of the spectra measured at different temperatures. Thus, the band designation and origin correspond to those accepted in the previous section. It was found that the low-temperature spectra of the 22Cs samples are well reproduced by the same set of partial bands as the glass spectra. However, the low-temperature set of partial bands is insufficient for modeling of the high-temperature spectra, and a new H5 component appears in deconvolution of these spectra. One more H6 line appears in the modeling of the spectra of the sample with the highest Cs_2O content (37Cs). Both H5 and H6 bands were assigned to the Q^2 units. The H6 line is more likely due to $Q^{2,22}$ groups according to Figures 8(a) and 8(b).

The $[Q^n](T)$ dependences calculated according to system (7) are summarized in Table 1 (an additional item, I_{H6}, was added to the denominator of the last equation of system (7) in the calculation of the local structure of the 37Cs sample). According to the obtained data, the local structure of the studied glasses does not change under a moderate increase in temperature. Further increases in temperature lead to a decrease in the concentration of Q^3 species and an increase in concentrations of Q^4 and Q^2 units. These changes can be explained by the shift of the equilibrium,

$$2Q^3 \Longleftrightarrow Q^4 + Q^2, \tag{8}$$

to the right with increasing temperature.

The temperature of the beginning of the shift of equilibrium (8) to the right depends on the sample composition and most likely corresponds to the glass-transition (T_g) temperature. The dynamic equilibrium (8) is "frozen" at temperatures below T_g.

The $[Q^n]$ data can be used to determine the ΔH enthalpy of the reaction (8). The equilibrium constant of the

Table 1: The peak positions (cm^{-1}), relative intensities, and fractions of Q^n species (%) in investigated glasses and melts.

T, K	H1 (H1*)	H2 (H2*)	H3	H4	H5	H6	$[Q^4]$	$[Q^3]$	$[Q^2]$
				17%Cs_2O-83%SiO_2					
293	1008/0.020	1060/0.072	1098/0.325	1144/0.583	—	—	59	41	—
				22%Cs_2O-78%SiO_2					
293	1010/0.020	1065/0.068	1100/0.352	1145/0.560	—	—	44	56	—
473	1007/0.021	1063/0.074	1099/0.328	1142/0.577	—	—	44	56	—
683	1006/0.019	1060/0.074	1097/0.333	1140/0.574	—	—	44	56	—
793	1006/0.025	1060/0.081	1096/0.323	1138/0.571	—	—	44	56	—
898	1006/0.031	1059/0.093	1095/0.315	1135/0.555	935/0.006	—	46/45	52/54	2/1
1003	1004/0.035	1059/0.108	1095/0.308	1133/0.540	937/0.009	—	46/45	52/54	2/1
1113	1004/0.038	1056/0.128	1092/0.304	1129/0.517	931/0.013	—	46/45	51/53	3/2
1223	1001/0.049	1053/0.143	1091/0.285	1127/0.500	926/0.023	—	47/47	49/50	4/3
1443	998/0.062	1052/0.167	1091/0.259	1124/0.479	920/0.033	—	48/48	47/48	5/4
1553	998/0.067	1050/0.191	1088/0.249	1123/0.452	922/0.041	—	49/49	45/46	6/5
				27%Cs_2O-73%SiO_2					
293	1006/0.024	1062/0.105	1097/0.361	1139/0.505	929/0.005	—	28/27	70/73	2/<1
573	1005/0.022	1062/0.144	1097/0.354	1137/0.474	932/0.006	—	28/27	70/73	2/<1
683	1005/0.022	1062/0.134	1096/0.350	1135/0.490	935/0.004	—	28/27	70/73	2/<1
793	1005/0.024	1060/0.155	1094/0.344	1133/0.469	936/0.008	—	28/27	70/72	2/1
898	1002/0.024	1060/0.151	1094/0.340	1129/0.477	932/0.008	—	28/27	70/72	2/1
1003	1003/0.026	1058/0.158	1092/0.335	1127/0.471	929/0.010	—	29/27	69/71	2/2
1113	1002/0.036	1057/0.168	1093/0.324	1125/0.452	926/0.020	—	30/29	66/68	4/3
1223	1000/0.044	1055/0.188	1092/0.307	1122/0.433	923/0.028	—	31/30	64/66	5/4
1338	1001/0.051	1055/0.194	1090/0.285	1120/0.428	920/0.042	—	32/32	61/63	7/5
1553	1000/0.070	1052/0.209	1088/0.237	1119/0.426	916/0.058	—	34/34	57/58	9/8
				33%Cs_2O-67SiO_2					
293	1001/0.042	1060/0.177	1103/0.569	1143/0.184	934/0.028	—	7/6	87/89	7/6
573	996/0.043	1059/0.177	1101/0.566	1141/0.183	930/0.031	—	7/6	86/89	7/6
683	992/0.042	1058/0.179	1098/0.563	1137/0.184	927/0.032	—	7/6	86/89	7/6
793	989/0.046	1057/0.188	1096/0.539	1134/0.193	925/0.034	—	8/7	85/87	8/7
898	988/0.043	1056/0.185	1094/0.548	1130/0.191	922/0.033	—	7/6	86/88	7/6
1003	989/0.056	1057/0.240	1092/0.434	1128/0.225	918/0.045	—	9/8	82/84	9/8
1113	991/0.064	1056/0.233	1095/0.412	1130/0.238	917/0.053	—	11/10	79/81	11/10
1223	992/0.075	1057/0.240	1096/0.374	1130/0.245	918/0.066	—	13/12	75/76	13/12
1338	989/0.093	1054/0.258	1092/0.299	1126/0.262	916/0.088	—	15/15	69/70	15/15
1443	990/0.123	1057/0.266	1089/0.243	1123/0.275	915/0.093	—	18/18	64/64	18/18
				37%Cs_2O-63%SiO_2					
293	1005/0.088	1063/0.189	1099/0.579	1136/0.055	928/0.089	—	<1	82/83	18/17
573	1006/0.089	1062/0.176	1099/0.586	1137/0.057	927/0.092	—	<1	81/82	18/18
1003	1001/0.086	1060/0.186	1095/0.553	1134/0.083	922/0.083	871/0.009	<1	82/83	18/17
1113	1004/0.113	1062/0.216	1092/0.439	1130/0.120	919/0.091	872/0.021	4/4	74/74	22/22
1223	998/0.117	1057/0.236	1089/0.409	1127/0.114	912/0.105	867/0.019	5/5	72/72	23/23
1338	994/0.125	1052/0.270	1085/0.344	1122/0.126	906/0.107	860/0.028	7/7	69/68	24/25
1443	991/0.134	1055/0.263	1086/0.308	1121/0.139	903/0.128	855/0.028	9/9	65/64	26/27

disproportional reaction (7) expressed using the concentrations of the Q^n units is defined as

$$K = \frac{\left[Q^4\right]\left[Q^2\right]}{\left[Q^3\right]^2}. \quad (9)$$

In turn, the ΔH enthalpy of equilibrium (8) is calculated from the Van't Hoff equation:

$$\Delta H = -R\frac{d\left(\ln K\right)}{d\left(1/T\right)}. \quad (10)$$

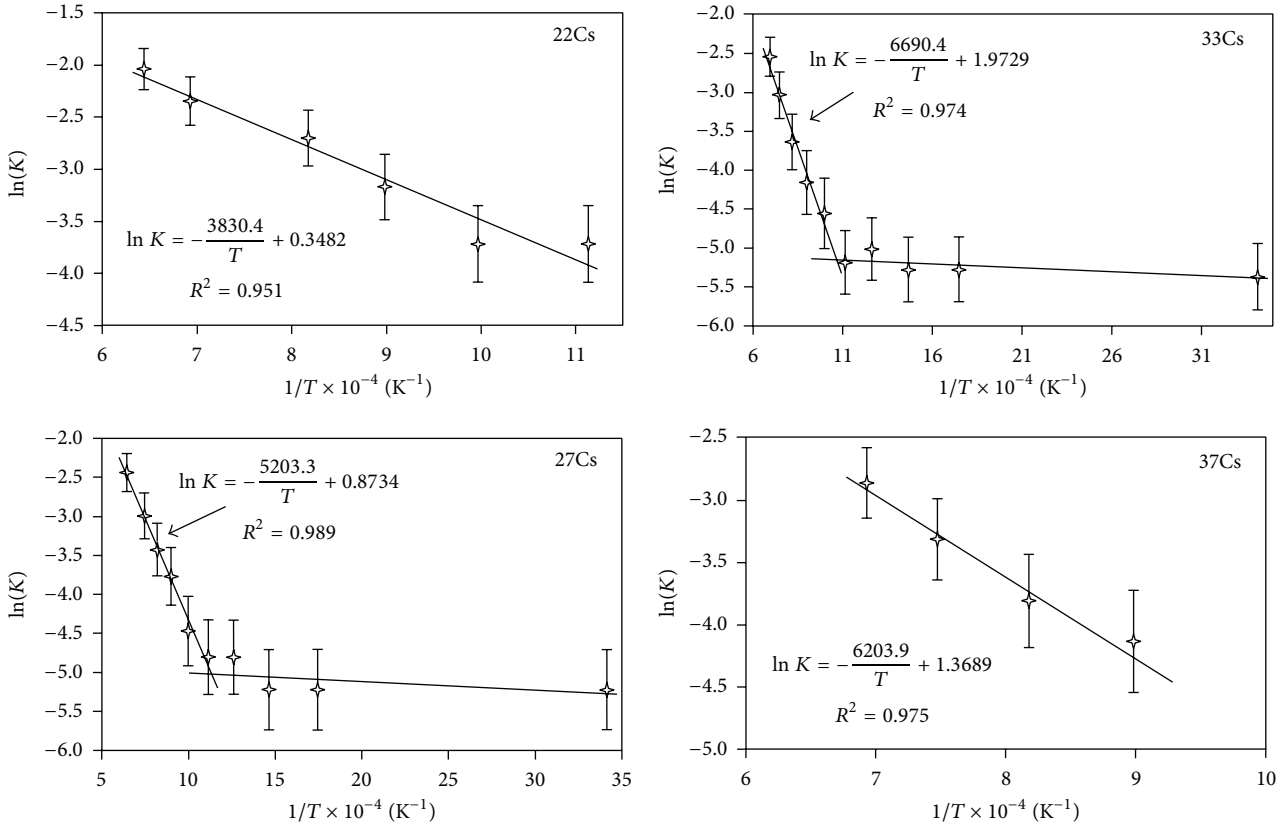

FIGURE 10: Relationship between equilibrium constant for equilibrium (7), $\ln K$, and $1/T$ (K^{-1}). The lines were obtained by least squares fitting.

Assuming that ΔH is independent of temperature above T_g, it is possible to calculate the enthalpy values using the slope of the $\ln(K)$ versus $(1/T)$ line from the high-temperature experimental data. The $\ln(K)(1/T)$ data are shown in Figure 10. Thus, the ΔH values for 22Cs, 27Cs, 33Cs, and 37Cs are obtained as 32 ± 6, 43 ± 8, 56 ± 10, and 52 ± 9 kJ/mol, respectively. These results show that ΔH value depends on the melt composition and is highest at 33 mol% Cs_2O. A similar trend has been observed for the sodium silicate system [8]. However, one should be advised and understand that there are a number of other reasons for decreasing of ΔH with increasing SiO_2 content: choice of the individual bands to modeling of poorly resolved high-frequency spectral envelope, Gaussian shape of individual peaks, an increase in experimental error at determination of the integral intensity of the weak bands ascribed to the Q^2 units, and so forth. Thus, we can assert unambiguously that ΔH is constant for the melts with x close to 33 mol% ($25 \le x \le 40$). Based on this conclusion one can see that there is a quite clear tendency for increase in ΔH with increasing alkali cation radius: ΔH is approximately equal to 0 [7, 37], 20 [11, 22, 37, 38], 30 [10, 39], and 50 kJ/mol (this work) for lithium, sodium, potassium, and cesium silicate melts, respectively.

Maehara et al. [8] have shown that $[Q^n]$ data can be used to calculate the nonideal entropy of mixing (ΔS_{mix}) for the silicate glasses and melts:

$$\Delta S_{\text{mix}} = -kA\left(\left[Q^2\right]\ln\left[Q^2\right] + \left[Q^3\right]\ln\left[Q^3\right] + \left[Q^4\right]\ln\left[Q^4\right]\right), \tag{11}$$

where $A = (1 - x/100)N_A$, N_A is the Avogadro constant, and k is Boltzmann's constant. As follows from Figure 6(a), the change in temperature does not significantly change the ΔS_{mix} in glasses and melts with high SiO_2 contents ($x < 20$ mol%). A similar situation would be typical for glasses with lower SiO_2 contents, but only at relatively low temperatures (less than T_g). As seen in Table 1, the local structure of the 22Cs, 27Cs, 33Cs, and 37Cs samples significantly changes at higher temperatures. Hence, considerable changes in ΔS_{mix} values are expected in this case. The ΔS_{mix} values as a function of temperature for the above-mentioned samples calculated by (11) are shown in Figure 11. As one can see, the entropy increases almost linearly with increasing temperature in the studied temperature range for all samples. The entropy change depends on the melt composition, the entropy increasing with modifier oxide content up to 33 mol% and then beginning to decrease.

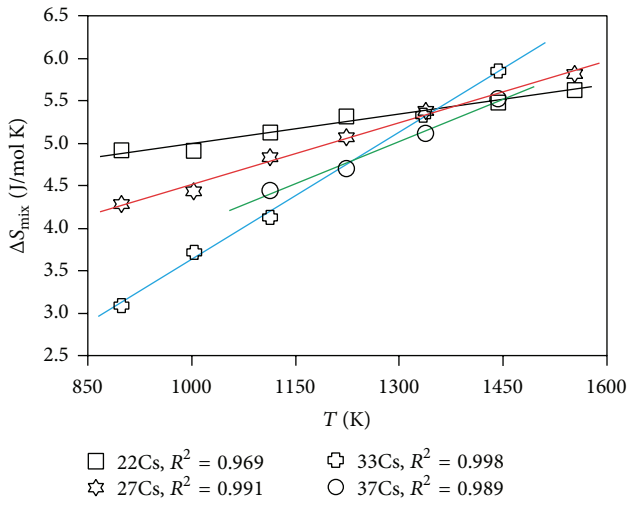

FIGURE 11: Plots ΔS_{mix} versus T for compositions indicated. Regression lines are through solid data points (above glass-transition interval).

5. Conclusion

The structure of the $x Cs_2O$-$(100 - x)SiO_2$ glasses and melts was studied by high-temperature Raman spectroscopy. It was found that the concentration of Q^4 species gradually decreases with increasing modifier oxide content. In turn, the fraction of Q^3 units increases, reaches a maximum at $x = 33$ mol%, and then starts to decrease. The Q^2 species are observed in the glass structure at $x \geq 27$ mol%. Their concentration increases with increasing Cs_2O content. The concentrations of Q^4 and Q^2 units are higher in the melt structure than in the corresponding glasses. The increase in the concentration of these structural units is explained by the shift of equilibrium (8) to the right with increasing temperature. The enthalpy of equilibrium (8) depends on the melt composition and was found to be equal to 32 ± 6, 43 ± 8, 56 ± 10, and 52 ± 9 kJ/mol for 22Cs, 27Cs, 33Cs, and 37Cs, respectively. The nonideal entropy of mixing, ΔS_{mix}, depends on the melt composition and increases linearly with increasing temperature at $T > T_g$. The $\Delta S_{mix}/\Delta T$ value also depends on the melt composition, increasing with the Cs_2O content up to 33 mol% and then beginning to decrease.

The $[Q^n]$ experimental data were used to model the Q^n distribution in Cs_2O-SiO_2 glasses and melts. The developed approach allows us to describe the experimental data over a wide composition range for both glasses and melts. The configurations of the random linkages generated during the modeling were analyzed for the identification of Q^i–Q^j and $Q^{n,ijkl}$ distributions. The results support the assumption that temperature changes weakly influence the Q^i–Q^j and $Q^{n,ijkl}$ distributions at relatively low Cs_2O contents (less than 15 ÷ 20 mol%). At higher Cs_2O contents, Q^i–Q^j bridges with $i = j$ are most sensitive to temperature. The direction of the change (increase/decrease) in concentration of the bridging bonds between one-type structural units depends on the glass (melt) composition, except for Q^4–Q^4 bridges, the concentration which always increases with increasing temperature at $x >$ 20 mol%. As for the $Q^{n,ijkl}$ groups, it was found that increasing temperature widens the variety of coexisting $Q^{n,ijkl}$ groups in the melt. The greatest change in the distribution of $Q^{4,ijkl}$ and $Q^{3,ijk}$ groups is expected in melts with $x \approx 33$ mol%, whereas the $Q^{2,ij}$ and $Q^{1,i}$ distributions are more prone to changes in the melts with $x \approx 50$ mol%.

Conflict of Interests

The authors declare that there is no conflict of interests regarding the publication of this paper.

Acknowledgment

Partial support by the RFBR (Project no. 14-08-00323_a) is gratefully acknowledged.

References

[1] R. Dupree, D. Holland, and D. S. Williams, "The structure of binary alkali silicate glasses," *Journal of Non-Crystalline Solids*, vol. 81, no. 1-2, pp. 185–200, 1986.

[2] H. Maekawa, T. Maekawa, K. Kawamura, and T. Yokokawa, "The structural groups of alkali silicate glasses determined from ^{29}Si MAS-NMR," *Journal of Non-Crystalline Solids*, vol. 127, no. 1, pp. 53–64, 1991.

[3] V. N. Bykov, A. A. Osipov, and V. N. Anfilogov, "Structural study of rubidium and caesium silicate glasses by Raman spectroscopy," *Physics and Chemistry of Glasses*, vol. 41, no. 1, pp. 10–11, 2000.

[4] W. J. Malfait, "Quantitative Raman spectroscopy: speciation of cesium silicate glasses," *Journal of Raman Spectroscopy*, vol. 40, no. 12, pp. 1895–1901, 2009.

[5] B. O. Mysen and J. D. Frantz, "Raman spectroscopy of silicate melts at magmatic temperatures: Na_2O-SiO_2, K_2O-SiO_2 and Li_2O-SiO_2 binary composition in the temperature range 25-1475 C," *Chemical Geology*, vol. 96, no. 3-4, pp. 321–332, 1992.

[6] J.-L. You, G.-C. Jiang, H.-Y. Hou, H. Chen, Y.-Q. Wu, and K.-D. Xu, "Quantum chemistry study on superstructure and Raman spectra of binary sodium silicates," *Journal of Raman Spectroscopy*, vol. 36, no. 3, pp. 237–249, 2005.

[7] V. N. Bykov, O. N. Koroleva, and A. A. Osipov, "Structure of silicate melts: Raman spectroscopic data and thermodynamic simulation results," *Geochemistry International*, vol. 47, no. 11, pp. 1067–1074, 2009.

[8] T. Maehara, T. Yano, and S. Shibata, "Structural rules of phase separation in alkali silicate melts analyzed by high-temperature Raman spectroscopy," *Journal of Non-Crystalline Solids*, vol. 351, no. 49-51, pp. 3685–3692, 2005.

[9] W. E. Halter and B. O. Mysen, "Melt speciation in the system Na_2O-SiO_2," *Chemical Geology*, vol. 213, no. 1–3, pp. 115–123, 2004.

[10] W. J. Malfait, V. P. Zakaznova-Herzog, and W. E. Halter, "Quantitative Raman spectroscopy: principles and application to potassium silicate melts," *Journal of Non-Crystalline Solids*, vol. 353, no. 44–46, pp. 4029–4042, 2007.

[11] W. J. Malfait, V. P. Zakaznova-Herzog, and W. E. Halter, "Quantitative Raman spectroscopy: speciation of Na-silicate glasses and melts," *American Mineralogist*, vol. 93, no. 10, pp. 1505–1518, 2008.

[12] B. O. Mysen and J. D. Frantz, "Silicate melts at magmatic temperatures: in-situ structure determination to 1651°C and effect of temperature and bulk composition on the mixing behavior of structural units," *Contributions to Mineralogy and Petrology*, vol. 117, no. 1, pp. 1–14, 1994.

[13] J. D. Frantz and B. O. Mysen, "Raman spectra and strucuture of $BaO\text{-}SiO_2$, $SrO\text{-}SiO_2$ and $CaO\text{-}SiO_2$ melts to 1600° C," *Chemical Geology*, vol. 121, no. 1–4, pp. 155–176, 1995.

[14] P. F. McMillan, G. H. Wolf, and B. T. Poe, "Vibrational spectroscopy of silicate liquids and glasses," *Chemical Geology*, vol. 96, no. 3-4, pp. 351–366, 1992.

[15] N. Umesaki, M. Takahashi, M. Tatsumisago, and T. Minami, "Raman spectroscopic study of alkali silicate glasses and melts," *Journal of Non-Crystalline Solids*, vol. 205-207, no. 1, pp. 225–230, 1996.

[16] L. Olivier, X. Yuan, A. N. Cormack, and C. Jäger, "Combined ^{29}Si double quantum NMR and MD simulation studies of network connectivities of binary $Na_2O{\cdot}SiO_2$ glasses: new prospects and problems," *Journal of Non-Crystalline Solids*, vol. 293–295, no. 1, pp. 53–66, 2001.

[17] O. Gedeon, M. Liška, and J. Macháček, "Connectivity of Q-species in binary sodium-silicate glasses," *Journal of Non-Crystalline Solids*, vol. 354, no. 12-13, pp. 1133–1136, 2008.

[18] J. Machacek and O. Gedeon, "Group connectivity in binary silicate glasses: a quasi-chemical approach and molecular dynamics simulation," *Journal of Non-Crystalline Solids*, vol. 354, no. 2-9, pp. 138–142, 2008.

[19] J. Du and A. N. Cormack, "The medium range structure of sodium silicate glasses: a molecular dynamics simulation," *Journal of Non-Crystalline Solids*, vol. 349, pp. 66–79, 2004.

[20] D. Sprenger, H. Bach, W. Meisel, and P. Gütlich, "Discrete bond model (DBM) of sodium silicate glasses derived from XPS, Raman and NMR measurements," *Journal of Non-Crystalline Solids*, vol. 159, no. 3, pp. 187–203, 1993.

[21] V. N. Bykov, A. A. Osipov, and V. N. Anfilogov, "High-temperature device for registration of Raman spectra of melts," *Rasplavy*, no. 4, pp. 28–31, 1997 (Russian).

[22] V. N. Anfilogov, V. N. Bykov, and A. A. Osipov, *Silicate Melts*, Nauka, Moscow, Russia, 2005.

[23] A. A. Osipov and L. M. Osipova, "Structure of lithium borate glasses and melts: investigation by high temperature Raman spectroscopy," *Physics and Chemistry of Glasses: European Journal of Glass Science and Technology Part B*, vol. 50, no. 6, pp. 343–354, 2009.

[24] W. H. Zachariasen, "The atomic arrangement in glass," *Journal of the American Chemical Society*, vol. 54, no. 10, pp. 3841–3851, 1932.

[25] A. A. Osipov and L. M. Osipova, "Q^n distribution in silicates: alkali silicate glasses and melts," *Advanced Materials Research*, vol. 560-561, pp. 254–258, 2012.

[26] A. A. Osipov and L. M. Osipova, "New approach to modeling of a local structure of silicate glasses and melts," *Journal of Physics: Conference Series*, vol. 410, no. 1, Article ID 012019, 2013.

[27] W. J. Malfait, W. E. Halter, Y. Morizet, B. H. Meier, and R. Verel, "Structural control on bulk melt properties: single and double quantum ^{29}Si NMR spectroscopy on alkali-silicate glasses," *Geochimica et Cosmochimica Acta*, vol. 71, no. 24, pp. 6002–6018, 2007.

[28] B. Boizot, S. Agnello, B. Reynard, R. Boscaino, and G. Petite, "Raman spectroscopy study of β-irradiated silica glass," *Journal of Non-Crystalline Solids*, vol. 325, no. 1–3, pp. 22–28, 2003.

[29] R. J. Hemley, H. K. Mao, P. M. Bell, and B. O. Mysen, "Raman spectroscopy of SiO_2 glass at high pressure," *Physical Review Letters*, vol. 57, no. 6, pp. 747–750, 1986.

[30] F. Ruiz, J. R. Martínez, and J. González-Hernández, "A simple model to analyze vibrationally decoupled modes on SiO_2 glasses," *Journal of Molecular Structure*, vol. 641, no. 2-3, pp. 243–250, 2002.

[31] S. K. Sharma, T. F. Cooney, Z. Wang, and S. van der Laan, "Raman band assignments of silicate and germanate glasses using high-pressure and high-temperature spectral data," *Journal of Raman Spectroscopy*, vol. 28, no. 9, pp. 697–709, 1997.

[32] V. Martinez, C. Martinet, B. Champagnon, and R. Le Parc, "Light scattering in $SiO_2\text{-}GeO_2$ glasses: quantitative comparison of Rayleigh, Brillouin and Raman effects," *Journal of Non-Crystalline Solids*, vol. 345-346, pp. 315–318, 2004.

[33] D. W. Matson, S. K. Sharma, and J. A. Philpotts, "The structure of high-silica alkali-silicate glasses. A Raman spectroscopic investigation," *Journal of Non-Crystalline Solids*, vol. 58, no. 2-3, pp. 323–352, 1983.

[34] P. McMillan, "Structural studies of silicate glasses and melts—applications and limitations of Raman spectroscopy," *American Mineralogist*, vol. 69, no. 7-8, pp. 622–644, 1984.

[35] B. G. Parkinson, D. Holland, M. E. Smith et al., "Quantitative measurement of Q^3 species in silicate and borosilicate glasses using Raman spectroscopy," *Journal of Non-Crystalline Solids*, vol. 354, no. 17, pp. 1936–1942, 2008.

[36] T. Furukawa, K. E. Fox, and W. B. White, "Raman spectroscopic investigation of the structure of silicate glasses. III. Raman intensities and structural units in sodium silicate glasses," *The Journal of Chemical Physics*, vol. 75, no. 7, pp. 3226–3237, 1981.

[37] B. O. Mysen and J. D. Frantz, "Structure and properties of alkali silicate melts at magmatic temperatures," *European Journal of Mineralogy*, vol. 5, no. 3, pp. 393–407, 1993.

[38] V. N. Bykov, A. A. Osipov, and V. I. Anfilogov, "Raman spectroscopy of melts and glasses in $Na_2O\text{-}SiO_2$ system," *Rasplavy*, no. 6, pp. 86–91, 1998 (Russian).

[39] V. N. Bykov, O. N. Koroleva, and A. A. Osipov, "Structure of $K_2O\text{-}SiO_2$ melts: Raman spectroscopic data and thermodynamic simulation results," *Rasplavy*, no. 3, pp. 50–59, 2008 (Russian).